Predicting the post-impact velocity of a robotic arm

Ilias Aouaj, Vincent Padois, Alessandro Saccon

Predicting the post-impact velocity of a robotic arm

Ilias Aouaj[1], Vincent Padois[2], Alessandro Saccon[3*]

***Abstract*— Starting from the recorded dynamic response of a 7DOF torque-controlled robot while intentionally impacting a rigid surface, we investigate the possibility of predicting the post-impact robot velocity from the ante-impact velocity and configuration. The velocity prediction is obtained by means of an impact map, derived using the framework of nonsmooth mechanics, that makes use of the known rigid-body robot model and the assumption of a frictionless inelastic impact. The main contribution is proposing a methodology that allows for a meaningful quantitative comparison between the recorded post-impact data, that exhibits a damped oscillatory response after the impact, and the post-impact velocity prediction derived via the rigid-body robot model, that presents no oscillations. The results of this approach are promising and the recorded impact data (18 experiments) is made publicly available, together with the numerical routines employed to generate the quantitative comparison, to further stimulate research in this field.**

I. INTRODUCTION

Robot manipulation tasks are typically performed by establishing contact at almost-zero velocity [1]. While this strategy is generally effective and provides some weak guarantees regarding the success of the task, it increases its execution time as well as the energy expenditure (due to the associated acceleration/deceleration phases required to bring the contact velocity to zero) when compared with a scenario where contact is established at non-zero velocity. As modern (torque controlled) robots are now being designed for dynamical physical interaction, it is necessary to develop in parallel a modeling framework able to capture the essence of contact interactions at non-zero speed. Such a framework will serve as basis for new control, learning, planning, and sensing strategies [2], [3].

Establishing contact at non-zero velocity leads to impact/collisions, rapid changes in the system velocities, and short-lived vibrations. The development of impact models is steadily gaining importance in the robotics community [4], together with the need for validation of these models against real experiments to assess their prediction ability and range of applicability [5]. Robot-environment collision models have a long history in robotics [6], [7], [8]. Early examples of impact modeling in robotics also include [9] and [10]. Despite this long history, existing publications concerning experimental validation of impact maps are currently limited to robot locomotion [11], single free-falling objects (typically, lightweight small spherical objects, cylinders, or dumbbells) impacting a rigid surface or a robot manipulator, but with without affecting its dynamics [12]. We are also unaware of publicly available robot-object-environment impact motion databases. Acknowledging the emergence of robots capable of controlled physical interactions, the aim of our investigation is instead that of *impact aware manipulation*: we envision robots grabbing and pushing massive objects that have a fast and direct influence on the robot dynamics right after contact is established.

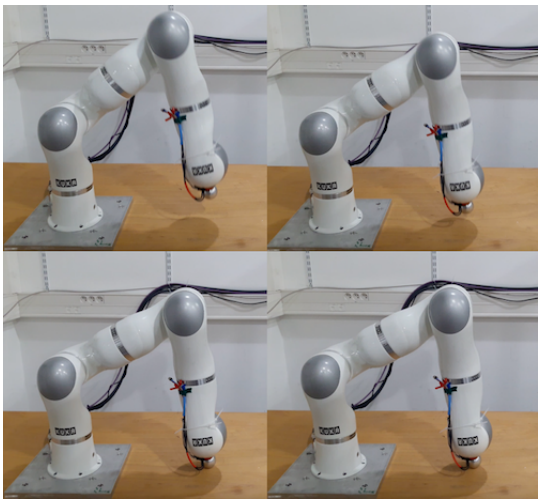

Fig. 1. Example of a vertical impact test at 0.2 m/s conducted on a KUKA LWR IV+ robotic arm. The figure shows four snapshots from a recorder video. Time evolves from left to right, from top to bottom.

The aim of this paper is to contributes fill in some of these identified gaps in the literature, first by making available[1] the joint data of the torque controlled robotic arm while impact a wooden table at different speed and impact angle (see Figure 1 for an illustration of this impact scenario) and then proposing a framework for quantitatively assessing the prediction ability of an impact map derived from a known rigid body robot model in determining the post-impact robot velocity.

As known from the field of nonsmooth mechanics, the impact map is the result of the combination of an impact equation and an impact law. For a robot manipulator, the impact equation is derived from an identified rigid body model (typically deriving directly from 3D CAD drawings). When performing impact experiments, however, visible oscillatory transients are visible: in our experiments, these last for about a hundred milliseconds. At first, it is unclear how to assess the post-impact prediction

This work was partially supported by the Research Project I.AM. through the European Union H2020 program under GA 871899.

[1]Ilias Aouaj has conducted this work during his MSc project at the Department of Mechanical Engineering, Eindhoven University of Technology (TU/e), The Netherlands (aouajilias@gmail.com)

[2]Vincent Padois is with Inria, Centre Bordeaux Sud-Ouest, Équipe AUCTUS Inria / IMS (Univ. Bordeaux, CNRS UMR5218), F-33405 Talence, France (vincent.padois@inria.fr)

[3*]Alessandro Saccon (corresponding author) is with the Department of Mechanical Engineering, Eindhoven University of Technology (TU/e), The Netherlands (a.saccon@tue.nl)

[1]The impact data and associated MATLAB scripts (that make use of the Robotics Toolbox [13] for handling of the robot kinematics), can be downloaded from the following URL: www.dct.tue.nl/asaccon/impact_dataset.zip.

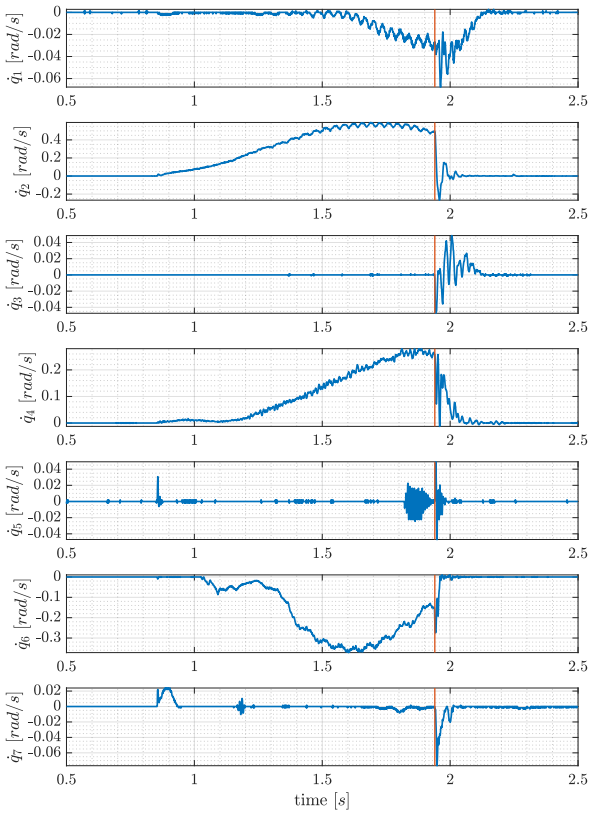

Fig. 2. Joint velocity signals for an impact at 0.2 m/s and 90deg with respect to the horizontal table. The vertical red line corresponds to the estimated impact time. Joint velocities are obtained via centered finite difference of the recorder encoder data (each subplot has a different scale to make the effect of the impact evident).

performance of an impact map derived from an idealized rigid-body robot model with an idealized algebraic impact laws versus the measured impact response. The main contribution of this work is to propose a methodology to separate the rigid response from the oscillatory response of the robot and consequently a methodology to assess the quality of the post-impact prediction. The procedure is illustrated first on an academic example and then applied on the recorded impact data of a 7DOF robotic arm, showing good prediction capability.

The paper is organized as follows. Besides this introduction, Section II provides basic background information regarding non-smooth mechanics and impact maps. A description of the impact experiments and problem statement is provided in Section III. Section IV details the main contribution, which is first introduced for an easily accessible academic example. Application of the proposed methodology on the 7DOF robot data is presented in Section V. Finally, conclusions and future work is discussed in Section V.

II. NONSMOOTH MECHANICS IMPACT MAPS

Within dynamical systems theory, nonsmooth mechanics [14] is quite a mature theoretical framework that combines rigid body modeling with algebraic impact laws, with the aim of capturing the post-impact state of a mechanical system based on the ante-impact configuration and velocity. The essential modeling assumption within this framework is a space-and-time scale separation between the contact and body dynamics that justifies approximating the impact dynamics as instantaneous (i.e., taking zero time) and consequently allowing for instantaneous jumps in the system's velocity and corresponding impulsive contact forces.

While admitting instantaneous velocity jumps and impulsive contact forces is a clear idealization of the contact dynamics (for the family of robots we are considering in this work, impact duration is typically in the range of 5 to 10 ms as shown in [15], [16], [17]), advanced impact models can provide impressive prediction capabilities even in the presence of multiple simultaneous impacts [18]. Also, these algebraic impact models have demonstrated extremely effective in planning and control for systems undergoing impacts, going from the estimation of the distribution of possible poses of a known object dropped on a surface from an arbitrary height [19], model-based dynamic robot locomotion [20], [21], and accurate batting of flying objects [12]. There is therefore good hope that similar models, once validated, can be also of great use in impact aware robot manipulation.

In the simplest form assumed in this paper, the *impact map* (i.e., the post-impact velocity prediction) is obtained starting from the standard equations of motion

$$M(q)\ddot{q} + h(q,\dot{q}) = \tau + J_N^T(q)\lambda_N, \qquad \text{if } g_N(q) = 0, \tag{1}$$

$$M(q)\ddot{q} + h(q,\dot{q}) = \tau, \qquad \text{if } g_N(q) > 0, \tag{2}$$

where $q \in \mathbb{R}^n$ is the generalize coordinates, M the mass matrix, h the Coriolis and gravity terms, τ the actuation torque, g_N the *gap function* representing the distance between the robot and the surface, $J_N(q) \in \mathbb{R}^{1\times n}$ the corresponding Jacobian, and $\lambda_N \in \mathbb{R}$ is the normal contact force. In nonsmooth mechanics, λ_N is allowed to become impulsive at the moment of collision and this leads to the so-called *impact equation* [14]

$$M(q)(\dot{q}^+ - \dot{q}^-) = J_N^T(q)\Lambda_N, \tag{3}$$

where Λ_N represents the impulsive force magnitude and $\dot{q}^+$ and $\dot{q}^-$ denote the post- and ante-impact velocities, respectively. The impact map is obtained combining the impact equation with an *impact law* that in case of a frictionless inelastic impact as we consider in this work reads

$$\dot{g}_N^+ = J_N(q)\dot{q}^+ = 0. \tag{4}$$

The impact map allows for a velocity jump, while keeping the configuration unaltered. The combination of (3) and (4), leads to the following single-point frictionless inelastic *impact map* (valid for $g_N(q) = 0$)

$$\dot{q}^+ = \left(I - M(q)^{-1}J_N^T(J_N M^{-1} J_N^T)^{-1} J_N\right)\dot{q}^-. \tag{5}$$

In the presence of friction, partially elastic and/or multiple simultaneous impacts, the formulation of the impact map becomes necessarily more sophisticated [22] but this is not essential for transmitting the core message of this work and therefore left out.

III. PROBLEM STATEMENT

Several impact experiments have been conducted between a torque controlled robotic arm (KUKA LWR IV+) and a smooth wooden table (cf. Figure 1). The robot impacted the table via a spherical metal probe that was secured via bolts to the standard robot tool mounting plate. A representative example of the recorded joint angles during an impact experiment is given in Figure 2. In this particular experiment, the impact between the table and the robot is normal to the table and occurs at a

Cartesian velocity of 0.2 m/s, approximately at time 1.94 s. A post-impact damped vibratory response can be observed, lasting approximately 100 ms. Just the second, fourth, and six joints are notably affected by the impact: this is justified by the fact that the impact motion occur essentially on a vertical plane (2D motion), which is also an approximate plane of symmetry for the robot and in which the mentioned joints are the one that affect the arm motion the most (essentially, we are looking at a planar impact of a planar RRR manipulator).

Besides this particular experiment, various combinations of low impact velocities and angles have been recorded (about twenty experiments, with repetitions). Overall, the impact velocity varied between 0.1 and 0.2 m/s and the impact angle between 30 and 90 degrees with respect to the table surface.

The impact experiments were obtained employing a task-based QP robot controller[2] (cf. [23] and [24] and references therein). The control torques are computed based on 7DOF rigid-body kinematics, velocity kinematics and dynamic models obtained using the KDL library[3]. The controller is assigned a pose task for the end-effector (with a linear motion for the metal probe center with constant velocity and constant orientation) and a regularization task (constant joint posture) to avoid self motions. The goal pose is located below the wooden table and cannot be reached as impact with table occurs first. Once contact has been detected using torque measurements at the joint level, the controller switches to pure gravity compensation.

To validate the lack of influence of the controller in the impact response, different experiments have been performed where the Cartesian PD gains have been altered and checking that no appreciable difference in the post-impact response in the joint signals could be observed. This lead to hypothesize that the post-impact oscillations (cf. Figure 2) are of structural nature. A confirmation of this fact would require the mounting of accelerometers and accessing both motor and joint encorders on the robot: this is deemed as a future research but the observed oscillations are very likely due to joint level non-rigidities induced by the gears (Harmonic drive) of the transmission as well as the torque sensing technology. What is relevant for the discussion that follows is, in any case, that the system exhibits damped oscillatory modes whose time scale is of at least an order of magnitude higher than the impact phenomenon.

As anticipated in the introduction, the impact data reported in Figure 2 makes it apparent that there is a fundamental challenge when trying to employ a post-impact velocity prediction based on a rigid-body robot model. Post-impact predictions based on rigid-body models do not exhibit any oscillatory behavior after an impact and therefore it is unclear how their prediction can be validated against real impact experiments that present damped post-impact oscillatory transients. The challenge is therefore summarized in the following problem statement, for which we propose a solution in Section IV.

Problem statement. How can we quantitatively compare the experimental post-impact velocity data against the post-impact velocity estimate that can be readily obtained via an available rigid-body robot model and a algebraic impact law?

[2]https://github.com/kuka-isir/rtt_lwr/releases and https://orca-controller.readthedocs.io/

[3]https://github.com/orocos/orocos_kinematics_dynamics

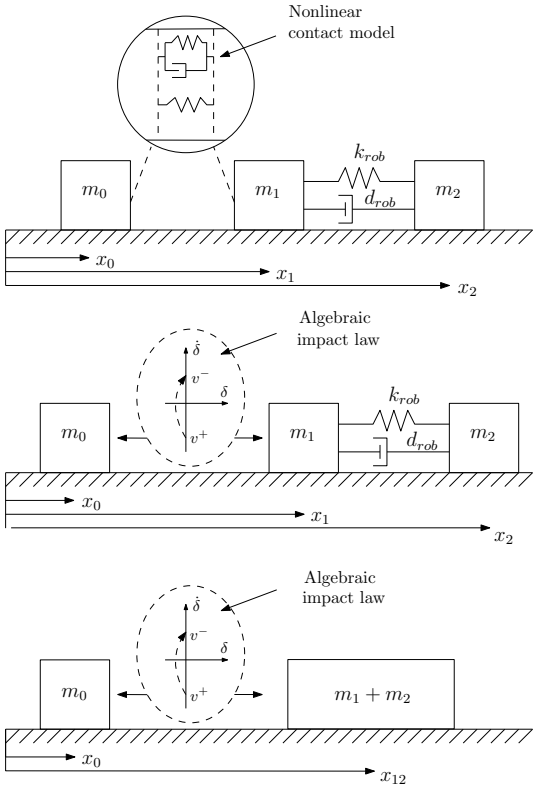

Fig. 3. Three levels of abstraction of an impact scenario, where a "1-DOF robot" (right) physically interacts with an external rigid object (left): (top) Contact is compliant and the robot is flexible; (middle) Contact is modelled via an algebraic impact law and the robot is flexible; (down) Contact is modelled via an algebraic impact law and the robot is rigid.

IV. CONTRIBUTION

In this section, we propose a procedure to assess the performance of the post-impact prediction obtainable with a rigid body impact model against the recorder impact data. At first, for illustration purposes, this procedure is introduced by means of an academic example employing two bodies colliding with each other along a straight line. We model these two bodies and the interaction between them in different ways, obtaining in total three different dynamical systems, as depicted in Figure 3. All these three models are made of an "interaction environment" (the body depicted on the left, considered fully rigid and with mass m_0) and a "robot" (the body depicted on the right, with total mass $m_1 + m_2$). The three models are detailed in the following bullets.

• **Model A: Compliant-contact/flexible-robot.** In this model, the robot (right) is assumed to be flexible and represented as the ensemble of two masses (m_1 and m_2) connected via a compliant coupling, with linear stiffness k_{rob} and damping d_{rob}. The interaction between the robot and the external object (left) is modeled via the well-known Hunt-Crossley nonlinear contact model [25], which relates the interpenetration g_N and its rate of change to the contact force F. Namely, we have

$$F(g_N, \dot{g}_N) = \begin{cases} k_{env}\, g_N^c + d_{env}\, g_N^c \dot{g_N}, & g_N \geq 0, \\ 0, & g_N < 0, \end{cases} \tag{6}$$

with k_{env}, d_{env}, and c chosen constants. Due to the interpenetration-dependent damping coefficient $d_{env}\ g_N^c$, the Hunt-Crossly contact model does not exhibit any (nonphysical)

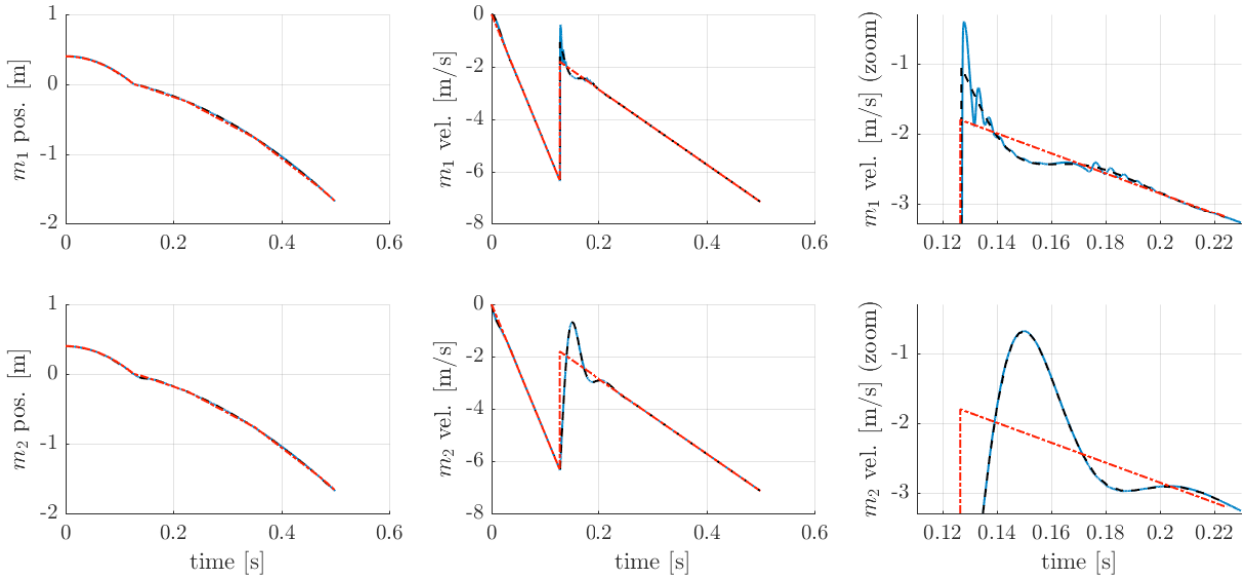

Fig. 4. Simulation results corresponding to the three models, where motion signals are given for mass m_1 and m_2. Model A is depicted in blue, Model B in dashed black, and Model C in dashdot red. The last column is a zoomed version of the middle column.

contact force jump when contact is established at non-zero velocity. In the simulations presented hereafter in this section, the damping coefficient is set to a very high value in order to simulate (almost) inelastic impacts;

• **Model B: Hard-contact/flexible-robot.** In this model, the contact interaction between the (flexible) robot is modelled via the fully inelastic impact law $\dot{\delta}^+ = \dot{x}_1^+ - \dot{x}_0^+ = 0$, triggered whenever $\delta := x_1 - x_0 = 0$ and $\dot{\delta}^- = \dot{x}_1^- - \dot{x}_0^- < 0$ ("+" and "−" denote left and right limits at impact time);

• **Model C: hard-contact/rigid-robot.** In this model, the robot is consider as a point mass (with mass $m_1 + m_2$) and the robot-environment contact is rigid (same impact law as in Model B).

Looking at these three models, it should be apparent that model A is the closest one to physical reality, while model C, based on rigid-body assumption, represents the one that is that is typically available and used for robot control and planning.

An illustrative numerical simulation of an impact. We consider the situation where the environment (m_0) and the robot (m_1 and m_2) start at rest and a constant force is applied to m_2. This force accelerates the robot towards the left until it impacts with the environment and a sudden velocity change is experienced, making the environment start moving and the robot to suddenly decelerate. In Figure 4, we report the corresponding motion of the robot for the three models described above, by showing the position and velocity signals of the two masses m_1 and m_2 (for model C, the motion of m_1 and m_2 are identical as they are rigidly connected).

TABLE I

PARAMETERS USED IN THE NUMERICAL SIMULATIONS

Parameter	Value	Units	Parameter	Value	Units
m_0	5	kg	m_1	1	kg
m_2	1	kg	c	3/2	[-]
k_{env}	$1 \cdot 10^8$	N/m^c	d_{env}	$1 \cdot 10^8$	Ns/m^{c+1}
k_{rob}	$1 \cdot 10^4$	N/m	d_{rob}	80	N s/m

Without loss of generality, the initial separation between m_0 and m_1 was set to 0.4 m and the constant pushing force to 100 N. The simulation parameters for the Hunt-Crossley model (k_{env}, d_{env}, and c) have been chosen based on the metal-wood interaction in the real robot-table experiment, assuming a stiffness corresponding to hard wood, a sphere-halfspace Hertz contact, and high damping to represent an impact with a small coefficient of restitution. The stiffness of the robot k_{rob} is chosen to be lower than the contact's and the damping d_{rob} to get a lightly damped response. Simulations were performed in MATLAB using the `ode15s` solver (a stiff ODE solver is used to deal with the stiff ODE related to high contact stiffness used in model A).

Discussion about the simulation results. The numerical results on Figure 4 show that the dynamic responses of robot in models A and B are essentially indistinguishable at the time scale of interest. This is simply an illustration of the time-and-space scale separation of contact and body dynamics, which justify the contact modeling simplification employed in nonsmooth mechanics. The zoomed-in version of the impact response of m_1 depicted in the last column of Figure 4 shows that the compliant and nonsmooth rigid contact models do indeed differ on a millisecond time scale, with the nonsmooth model B just capturing the average response of the compliant model A. The numerical simulation of model A shows explicitly two distinctive dynamics at work: one fast due to contact stiffness ($0.12 - 0.14$ s in the top subplot) and the one slower, captured also by model B ($0.12 - 0.21$ s and beyond). Inspection of the gap function actually shows bouncing of mass m_1 on m_0 before full adhesion. Other simulations with higher damping at contact (namely, $1 \cdot 10^9$ Ns/m^{c+1}), instead, show no bouncing between m_1 and m_0 and an even closer matching between the motions of mass m_1 for models A and B (these plots not reported for space limitation, but they are easily reproduced with the provided MATLAB script). Either with higher or lower contact damping, at the "actuation-and-sensing" side (m_2), the responses of model A and model B are

essentially indistinguishable (see bottom right plot in Figure 4).

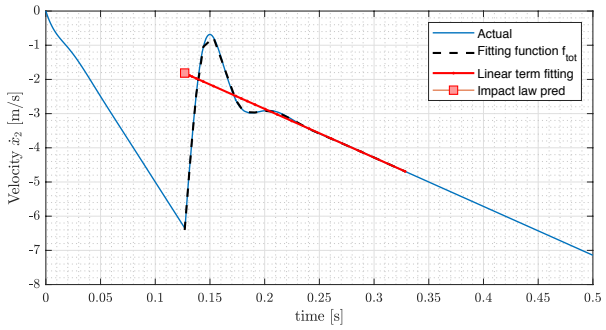

Fig. 5. Numerical data fitting result. Here we used the fitting scheme on the velocity signal of mass m_2, where the linear term of the fitting function is extrapolated back to the time instance of impact. In addition, the prediction of the post-impact velocity of the impact map is also provided, which is compared to the estimation provided by the extrapolation.

Key observation and contribution. At this point, it becomes interesting also to compare the behavior of model B (flexible robot) with that of model C (rigid robot). In particular, regarding the actuation-and-sensing side of the robot (m_2). Figure 4 illustrates that the velocity of the flexible robot model converges to that of the rigid robot model in about 100 ms, suggesting to interpret the response of the flexible robot model as that of a low-pass filter acting on a velocity step input. The flexible robot dynamics is thus seen also as a faster dynamics compared to that of the gross motion of the bodies composing the system. Given the time and space scales (in real experiments, these vibrations are only observable looking at encoder data), we suggest to treat the post-impact vibration dynamics as linear and thus as the superposition of exponentially decaying oscillatory responses (including constant and linear terms corresponding to a step input). Least square fitting/modal analysis techniques can be thus used to remove the oscillatory part of the post-impact time response, extracting just the steady state response (constant and linear term). An example of application of this procedure, where the velocity signal is decomposed into the sum of a constant, a linear function of time, and just one exponentially decaying function of the form $A\exp(\omega t+\phi)$ is given in Figure 5.

Proposed quantitative comparison procedure. Summarizing, we propose the following procedure to quantitatively compare the experimental post-impact data with the post-impact velocity prediction derived from a rigid-body impact map:

1) Identify the impact time t_i in the experimental data by looking at, e.g., sharp variations of joint encoder data (see [26] and references therein);
2) Extract the impact robot configuration $q(t_i)$ and corresponding pre-impact joint velocity $v^-(t_i)$ and compute the post-impact joint velocity estimate $\overset{\Delta}{v}{}^+(t_i)$ employing the impact map (5);
3) Use a (nonlinear) least square fitting (or frequency domain based) procedure to separate the affine (=constant plus linear) response from the oscillatory damped response ("sum of eigenmodes") over the interval $[t_i, t_i+T_s]$ where vibrations are observed (T_s denotes the chosen settling time). Employ the affine part to construct the virtual rigid robot post-impact velocity $\hat{v}^+(t_i)$;
4) Evaluate the (relative and absolute) error between $\overset{\Delta}{v}{}^+(t_i)$ and $\hat{v}^+(t_i)$ for impacts occuring at different postures and velocities, to quantify the general accuracy of the post-impact velocity estimation.

The result of applying this proposed comparison procedure on the 7DOF arms are reported in the following section.

V. FITTING RESULTS ON THE 7DOF ARM

Figure 6 illustrates the result of the fitting procedure described in the previous section for an impact at 0.2 m/s, and three different impact angles. Only vertical and horizontal Cartesian velocities are reported, as lateral displacement is negligible in the performed impact experiments as explained in Section III. The Cartesian velocities are obtained from the recorded joint velocities and the end-effector Jacobian. For the least square fitting, we employ for each signal the fitting function

$$f_{tot} = v^- + at + A\left(e^{\gamma t}\cos(\omega t+\phi)-\cos(\phi)\right) \qquad (7)$$

where t denotes the time after the impact t_i and v^- the pre-impact velocity. The five optimizing parameters for the least square fitting are the slope a, the amplitude A, the decay factor γ, the frequency ω, and the phase shift ϕ. More precisely, the full set of parameters is only used for the vertical Cartesian direction (which has a dominant second order response) while for fitting of the other signal, the frequency and decay rate are set equal to the one identified for the second Cartesian direction of interest in order to obtain a single real eigenmode. The fitting procedure is applied on a 150 ms time window, that was selected based on the stabilization of the least square fitting parameters and roughly corresponds to three oscillation periods. In the figure, the reconstructed ideal rigid response $v^- - A\cos(\phi)+at$ is shown as a red line. Its value $\hat{v}^+ = v^- - A\cos(\phi)$ at impact time should be compared with the the post-impact velocity estimate $\overset{\Delta}{v}{}^+$ (the red square in the plots), derived via the rigid-body impact map. The impact map is derived from the rigid-body robot model employed by the QP robot controller, combined with the frictionless inelastic impact law between the end-effector tip and the (assumed rigid) wooden table (as discussed in Section II).

Overall, the reconstructed and rigid-body impact map predictions, $\overset{\Delta}{v}{}^+$ and $\hat{v}^+$, show a remarkably good agreement. As summarized in Table II, this holds no just for the 0.2 m/s impacts, but also for the impact experiments at 0.15 m/s and 0.1 m/s. The tables shows the absolute prediction error $\eta := |\overset{\Delta}{v}{}^+ - \hat{v}^+|$ for both the normal and horizontal velocities is also shown (m/s). On average, we get a 8 mm/s absolute error and 7.3% relative error on predicting post-impact sliding velocity (the relative error is computed as $2|\overset{\Delta}{v}{}^+ - \hat{v}^+|/|\overset{\Delta}{v}{}^+ + \hat{v}^+|$).

Looking at the measured impact response, it is noticeable that the assumption of a second order system type response is only partially valid and higher frequency modes currently not modeled are present. This is more noticeable at the joint level (results are reproducible with the provided MATLAB scripts) and therefore we have chosen here to limit the model analysis based on a single mode of vibration at Cartesian level. The use of a more sophisticated modal analysis procedure at joint level is considered as the next step of our investigation.

VI. CONCLUSIONS

For the considered impact experiments between a 7DOF torque-controlled robotic arm with a wooden table, the post-

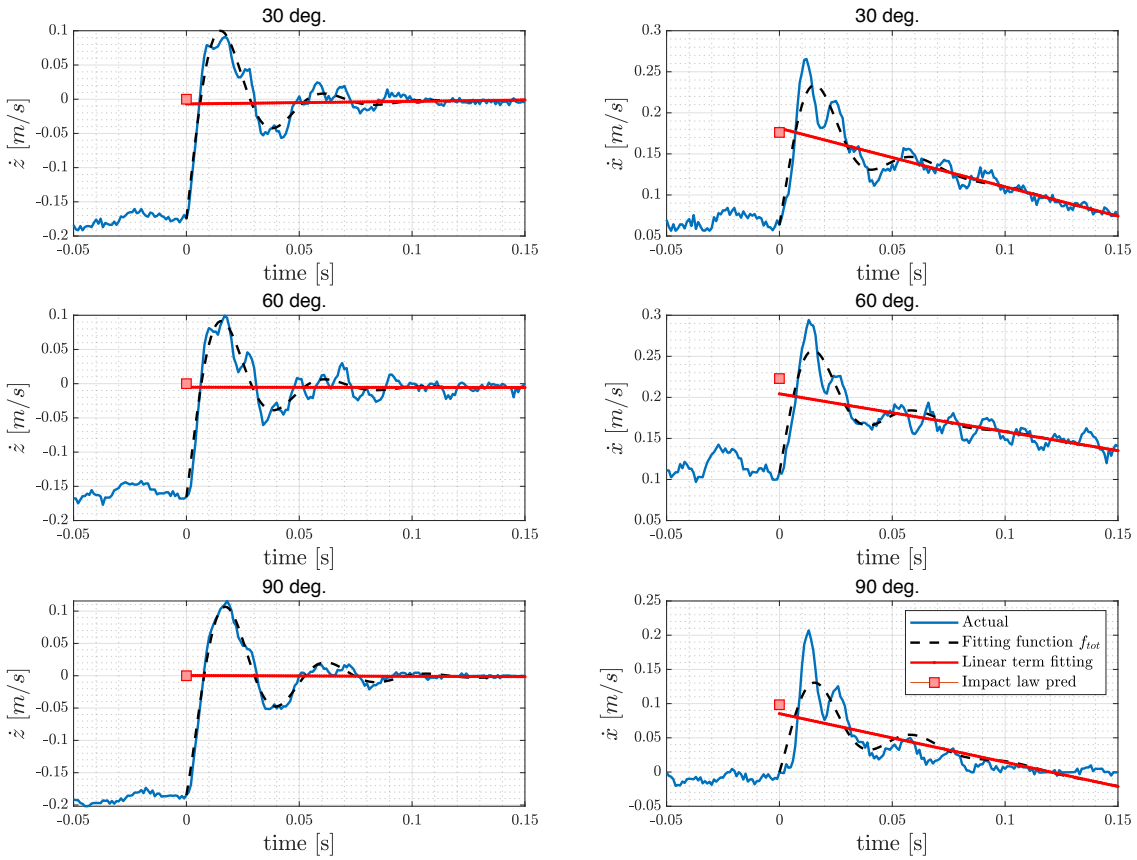

Fig. 6. Cartesian velocity fitting results for impact at 0.2 m/s under angles ranging from 30 to 90deg w.r.t. to the horizontal table. The x-direction (right) is tangential to the table and the z-direction (left) is normal.

TABLE II

EVALUATION OF THE IMPACT MAP AND FITTING RESULTS FOR THE TWO EXPERIMENTAL DATA SETS (DATA IN m/s)

velocity, angle	$\tilde{v}_z^-$	$\overset{\Delta}{v}_z^+$	$\hat{v}_z^+$	η_z	$\tilde{v}_x^-$	$\overset{\Delta}{v}_x^+$	$\hat{v}_x^+$	η_x	$\tilde{v}_z^-$	$\overset{\Delta}{v}_z^+$	$\hat{v}_z^+$	η_z	$\tilde{v}_x^-$	$\overset{\Delta}{v}_x^+$	$\hat{v}_x^+$	η_x
0.10 m/s, 30°	-0.097	0	-0.006	0.006	0.031	0.094	0.096	0.002	-0.085	0	-0.007	0.007	0.061	0.120	0.112	0.008
0.10 m/s, 60°	-0.085	0	-0.009	0.009	0.061	0.122	0.109	0.013	-0.099	0	-0.003	0.003	0.028	0.088	0.094	0.006
0.10 m/s, 90°	-0.101	0	-0.005	0.005	0.004	0.055	0.050	0.006	-0.103	0	-0.003	0.003	-0.007	0.039	0.050	0.011
0.15 m/s, 30°	-0.175	0	-0.007	0.007	0.064	0.176	0.181	0.005	-0.120	0	-0.012	0.012	0.092	0.178	0.170	0.008
0.15 m/s, 60°	-0.114	0	-0.010	0.010	0.096	0.174	0.163	0.011	-0.137	0	-0.006	0.006	0.054	0.140	0.149	0.009
0.15 m/s, 90°	-0.148	0	-0.003	0.003	-0.006	0.072	0.064	0.008	-0.148	0	-0.002	0.002	0.002	0.072	0.072	0.000
0.20 m/s, 30°	-0.175	0	-0.007	0.007	0.064	0.176	0.181	0.005	-0.144	0	-0.011	0.011	0.120	0.222	0.209	0.013
0.20 m/s, 60°	-0.165	0	-0.005	0.005	0.108	0.223	0.204	0.019	-0.168	0	-0.004	0.004	0.086	0.190	0.190	0.000
0.20 m/s, 90°	-0.185	0	0.000	0.000	0.000	0.098	0.085	0.013	-0.178	0	-0.002	0.002	0.003	0.093	0.099	0.006

impact response in the vertical Cartesian domain clearly shows a dominant second-order-system type response to an impact. On the horizontal direction, the response is more complex and more advanced modal analysis techniques could be explored. Nevertheless, the least square fitting with a single osciallory mode shows very good fitting results, with 7.3% relative error and 8 mm/s absolute error different between the measured and predicted sliding velocity over a set of 18 experiments at different impact velocity and impact angles. Further research is needed to develop fitting models with more than just a single oscillatory mode superimposed to the affine (=constant+linear) steady state response. Once this is done, the analysis should be extended at the level of joint signals. Further research will consider oblique impacts with rough surfaces, to study the post-impact velocity predictability in the present of surface friction. It is expected that these validated impact models will allow to achieve better performance in impact aware robot control schemes.

ACKNOWLEDGMENTS

The authors want to thank the Institut des Systèmes Intelligents et de Robotique (ISIR) at Sorbonne Université and CNRS (Paris, France) for providing access to the KUKA LWR 4+ robot used in this study, Lucas Joseph for collecting the collision data, and Claude Lacoursière for valuable feedback on a preliminary draft of this document.

REFERENCES

[1] S.S.M. Salehian and A. Billard. A dynamical-system-based approach for controlling robotic manipulators during noncontact/contact transitions. IEEE Robotics and Automation Letters, 3(4):27382745, 2018.

[2] M. Rijnen, E. de Mooij, S. Traversaro, F. Nori, N. van de Wouw, A. Saccon, H. Nijmeijer, Control of humanoid robot motions with impacts: Numerical experiments with reference spreading control. IEEE International Conference on Robotics and Automation (ICRA), 4102-4107, 2017

[3] Y. Wang, A. Kheddar, Impact-Friendly Robust Control Design with Task-Space Quadratic Optimization, Robotics: Science and Systems (RSS), 2019

[4] M. Halm, M. Posa, Modeling and Analysis of Non-unique Behaviors in Multiple Frictional Impacts. Robotics: Science and Systems (RSS), 2019

[5] Nima Fazeli, Samuel Zapolsky, Evan Drumwright, Alberto Rodriguez, Fundamental Limitations in Performance and Interpretability of Common Planar Rigid-Body Contact Models. International Symposium of Robotic Research (ISRR), 2017.

[6] J. K. Mills, "Manipulator transition to and from contact tasks: a discontinuous control approach," IEEE International Conference on Robotics and Automation (ICRA), pp. 440-446, 1990

[7] D. Walker, Impact configurations and measures for kinematically redundant and multiple armed robot systems, IEEE Transactions on Robotics and Automation, vol. 10, no. 5, pp. 670-683, Oct. 1994.

[8] D. N. Nenchev and K. Yoshida, Impact analysis and post-impact motion control issues of a free-floating Space robot subject to a force impulse. IEEE Transactions on Robotics and Automation, vol. 15, no. 3, pp. 548-557, June 1999.

[9] Y.-F. Zheng and H. Hemami, Mathematical modeling of a robot collision with its environment, Journal of Field Robotics, vol. 2, no. 3, pp. 289307, 1985.

[10] Y. Hurmuzlu, D.B. Marghitu, Rigid Body Collisions of Planar Kinematic Chains with Multiple Contact Points, International Journal of Robotic Research, 13(1):82-92, 1994

[11] H.W. Park, K. Sreenath, J. W. Hurst, J.W. Grizzle, Identification of a Bipedal Robot With a Compliant Drivetrain: Parameter Estimation for Control Design. Control Systems Magazine, 31(2):63-88, 2011

[12] Y.-B. Jia, M. Gardner, X. Mu, Batting an in-flight object to the target. The International Journal of Robotics Research, 38(4), 451485, 2019

[13] P.I. Corke, Robotics, Vision & Control. Springer 2017

[14] B. Brogliato, Nonsmooth mechanics: models, dynamics and control. Third edition, Springer, 2016.

[15] S. Haddadin, A. Albu-Schffer, G. Hirzinger, Safety Evaluation of Physical Human-Robot Interaction via Crash-Testing. Robotics: Science and Systems (RSS), 217-224, 2007

[16] Requirements for safe robots: Measurements, analysis and new insights S Haddadin, A Albu-Schffer, G Hirzinger. The International Journal of Robotics Research, 28(11-12):1507-1527, 2009

[17] S. Haddadin, A. Albu-Schaffer, A. De Luca, G. Hirzinger, Collision detection and reaction: A contribution to safe physical human-robot interaction. IEEE/RSJ International Conference on Intelligent Robots and Systems (IROS), 3356-3363, 2008

[18] N.S. Nguyen, B. Brogliato, Comparisons of multiple-impact laws for multibody systems: Moreaus law, binary impacts, and the LZB approach. Advanced Topics in Nonsmooth Dynamics, 1-45, 2018.

[19] M. Moll, M.A. Erdmann, Manipulation of pose distributions. International Journal of Robotics Research, 21(3):277292, 2002

[20] J.W. Grizzle, C. Chevallereau, R.W. Sinnet, A.D. Ames, Models, feedback control, and open problems of 3D bipedal robotic walking. Automatica 50 (8), 1955-1988, 2014

[21] J. Reher, E. A. Cousineau, A. Hereid, C. M. Hubicki, A. D. Ames, Realizing dynamic and efficient bipedal locomotion on the humanoid robot DURUS, IEEE Int. Conf. on Robotics and Automation, pp. 17941801, 2016

[22] C. Glocker, An Introduction to Impacts. In Nonsmooth Mechanics of Solids, eds J.Haslinger and G.E. Stavroulakis, pp. 45-101, Springer, 2006

[23] L. Joseph and V. Padois and G. Morel. Towards X-ray medical imaging with robots in the open: safety without compromising performances. IEEE International Conference on Robotics and Automation, 6604-6610, 2018.

[24] L. Joseph and V. Padois and G. Morel. Experimental validation of an energy constraint for a safer collaboration with robots. International Symposium on Experimental Robotics, 2018.

[25] K. H. Hunt and F. R. E. Crossley, Coefficient of Restitution Interpreted as Damping in Vibroimpact. ASME Journal of Applied Mechanics, 42(2): 440445, 1975.

[26] M. Rijnen, A. Saccon, H. Nijmeijer, Motion Signals With Velocity Jumps: Velocity Estimation Employing Only Quantized Position Data. IEEE Robotics and Automation Letters, 3(2):1498-1505, 2018